Agricultural Water Management 259 (2022) 107238

Contents lists available at ScienceDirect

Agricultural Water Management

journal homepage: www.elsevier.com/locate/agwat

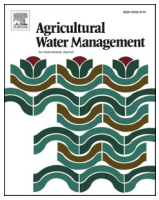

Joint analysis of drought and heat events during maize (*Zea mays* L.) growth periods using copula and cloud models: A case study of Songliao Plain

Ying Guo [a,b,c], Xiaoling Lu [e], Jiquan Zhang [a,b,c,*], Kaiwei Li [a,b,c], Rui Wang [d], Guangzhi Rong [a,b,c], Xingpeng Liu [a,b,c], Zhijun Tong [a,b,c]

[a] School of Environment, Northeast Normal University, Changchun 130024, China
[b] State Environmental Protection Key Laboratory of Wetland Ecology and Vegetation Restoration, Northeast Normal University, Changchun 130024, China
[c] Key Laboratory for Vegetation Ecology, Ministry of Education, Changchun 130024, China
[d] School of Chemisical and Environmental Engineering, Liaoning University of Technology, Jinzhou 121000, China
[e] School of Tourism and Geographic Sciences, Baicheng Normal College, Baicheng 137000, China

ARTICLE INFO

Handling Editor: Dr R Thompson

Keywords:
Concurrent events
High temperature
Climate change
Fuzziness
Randomness

ABSTRACT

Due to global warming, it is necessary to study the influence of extreme climate and concurrent events on crop growth. The study area was the Songliao Plain, where drought events frequently occur. First, the daily meteorological data of 14 meteorological stations from 1981 to 2016 were collected to analyze the temporal and spatial changes in the crop water surplus and deficit index, extreme growing degree-days, and heat stress intensity during different growth stages of maize. Second, the cloud model was used to describe the fuzziness of concurrent events (simultaneous drought and heat), and mutual mapping between qualitative and quantitative data was undertaken. The fuzzy certainty degree of the influence of different degrees of concurrent events on maize was calculated. Third, the copula function was used to describe the randomness of concurrent extreme events and calculate the joint probability distribution and return period. An assessment method was proposed for concurrent events from the perspective of system uncertainty. Finally, we analyzed the relationship between concurrent events and maize yield, which showed different degrees of water deficit and warming trends during each growth period. Crops were most affected by extreme weather during the reproductive growth period (RGP). During the vegetative growth period (VGP), the temperature increase was higher than in other periods, especially in the high-latitude region. The frequency of mild concurrent events was higher during the VGP and RGP. During the vegetative and reproductive period, the average occurrence probability of mild, moderate, and severe concurrent events was 21.9%, 1.7%, and 0.35%, respectively, whereas during the RGP, it was 23.1%, 8.2%, and 0.12%, respectively. The present study provides a meaningful reference for a better understanding of the occurrence laws of drought, heat, and concurrent events during crop growth periods and how to optimize the agricultural management of maize.

1. Introduction

In the past century, the Earth has experienced significant global warming (Lobell et al., 2011; Ray et al., 2019; Wang and Chen, 2014). After a record heat event in 2015, the World Meteorological Organization told the international community that it would need to cope with a hotter, drier, and wetter future (Church et al., 2013). Agriculture is particularly sensitive to climate change. Climatic factors, such as temperature, precipitation, radiation, and wind speed, affect the physiological development and yield of crops, and abnormal changes cause various agricultural disasters (Chen et al., 2016; Killi et al., 2017; Miliauskienė et al., 2016). Due to increasing global food demand, the temporal and spatial variation law of extreme weather and climate, and the occurrence law of concurrent agrometeorological disaster events must be identified. The present study will aid in making strategic decisions on food security and implementing policies, technologies, and strategies to adapt agriculture to climate change.

Drought is a natural agricultural disaster with a wide range, high

* Correspondence to: Northeast Normal University, 2555 Jingyue Street, Changchun City, Jilin Province, China.
E-mail addresses: guoy471@nenu.edu.cn (Y. Guo), zhangjq022@nenu.edu.cn (J. Zhang).

https://doi.org/10.1016/j.agwat.2021.107238
Received 2 June 2021; Received in revised form 17 September 2021; Accepted 4 October 2021
Available online 8 October 2021

frequency, and long duration that threatens national food security (Mahrookashani et al., 2017). Climate change has led to an increase in the severity and duration of drought events in many areas of China, often accompanied by heat and heat waves (Chen and Sun, 2017; Miao et al., 2016; Sun et al., 2014). Heat and drought are two related but different constraints. Although heat may not cause drought, it is likely to aggravate the degree of drought. The occurrence of drought is complex and lagging, whereas that of heat is short-term and sudden. Combining these two natural disasters will have a far-reaching effect on food security by shortening the crop growth period and reducing the crop production potential (Zandalinas et al., 2018). For example, in 2014, drought and a heat wave in California triggered wildfires and caused an agricultural water crisis (AghaKouchak et al., 2014). In 2016, there was historic heat and drought in Southeast Asia (Qian et al., 2019).

Research on the hazards and risks of the coexistence of various extreme meteorological events or agricultural disasters is limited (Leonard et al., 2014). Several studies have analyzed the challenges of the multi-hazard framework (AghaKouchak et al., 2014; Mesbahzadeh et al., 2020; Wang et al., 2019; Sharma and Mujumdar, 2017). The combined stress of heat and drought severely affects wheat yield compared to a single stress factor (Mahrookashani et al., 2017). Matiu et al. (2017) observed that maize yield decreased by 11.6% under dry and hot conditions but only by 7.8% under dry conditions using the standardized precipitation evapotranspiration index (SPEI) and temperature data. Lobell et al. (2015) reported that the effect of heat events is increasing, and heat factors should be considered when carrying out drought risk management. Thus, the traditional univariate risk assessment method based on precipitation conditions may significantly underestimate the risk of extreme events because it ignores the influence of temperature (Fang et al., 2019). Wang et al. (2018a) evaluated the risk of drought and heat events during the growth period of summer maize in the Huang-Huai-Hai Plain using SPEI during critical growth periods, combined with the cumulative distribution function and climate trend rate. Miao et al. (2016) comprehensively analyzed the joint probabilistic characteristics and tendencies for bivariate and trivariate precipitation and temperature indices based on the copula theory.

From previous studies, the relationship between meteorological factors and crop yield has been established based on deterministic methods or via model simulation and weight calculation using climatic factors. These ignore the uncertainty of the crop itself and the research system. Research on randomness and fuzziness of uncertain systems has advanced (Chen et al., 2012; Wu et al., 2019). However, few studies have combined the uncertainty study with a study of multiple extreme events. In the field of meteorological disasters, there are limited studies on the probability calculation of various extreme events. Therefore, it is essential to understand the temporal and spatial variation law of crop water requirement (ET_c), effective rainfall (P_{ei}), and extreme heat (heat stress intensity [HIS] and extreme growing degree-days [EDD]) during a maize growth period, and the occurrence of concurrent events of drought and heat in each period.

The primary purpose of the present study was to describe the randomness and fuzziness of drought and heat events on maize crops. The maize-producing area of the Songliao Plain was chosen as the study area. We combined the cloud and copula models to analyze two natural disasters together and answered the following questions based on uncertainty: (a) How do precipitation and extreme heat change during the different growth stages of maize? (b) What is the condition of concurrent drought-heat events in different degrees for maize in the study area? (c) How are the joint distribution probability and co-occurrence recurrence periods of compound stress distributed? The present study provided a meaningful reference for a better understanding of the occurrence laws of drought, heat, and concurrent events during the crop growth period and the results can aid in protecting fragile agro-ecosystems, which is of great significance for further study on hazard quantification and risk assessment of various agricultural disasters and the rational allocation of water and heat resources to ensure food security.

2. Study area and data sources

2.1. Study area

The Songliao Plain is located in northeast China, between 40°25′–48°40′ N and 118°40′–128°00′ E. It covers approximately 300 000 hm^2 in the southern Heilongjiang Province, central and western Jilin Province, and the majority of Liaoning Province. Located between the Daxing'an mountain range, Xiaoxing'an mountain range, and Changbai Mountain, it starts from the middle reaches of the Nenjiang River in the north and reaches the Liaodong Bay in the south (Fig. 1). The Songliao Plain is an important grain production base in China. During the 1970s, it gradually expanded and formed the current "maize belt" in China (Bai, 1998; Dao-Wei et al., 2010). The annual precipitation in the study area is 500–750 mm and the annual mean evaporation is 2–3 times that of the annual mean precipitation. The annual mean temperature is 3–8 ℃, the lowest temperature occurs in January, and the highest temperature occurs in July. The frost-free period is 135–155 d, and the annual average sunshine hours are 2400–2900 h. Due to various conditions, desalinated salt water and seawater cannot be applied for local agricultural production (Panagopoulos, 2021; Panagopoulos et al, 2019). Local water resources for agriculture are scarce, and the majority is cultivated from rain. The fertilization method is single, which is sensitive to environmental changes. Low temperatures in spring and frost in autumn are frequent, and natural disasters, such as drought and flood, are frequent (Guna et al., 2019; Zhang, 2004).

2.2. Data source

Based on the classification standard for the maize growth period, the present study divided the maize growth period into four stages: whole growth period (WGP), vegetative growth period (VGP), vegetative and reproductive period (VRP), and reproductive growth period (RGP). The WGP is defined from sowing to maturity, VGP is from sowing to jointing, VRP is from jointing to flowering, and RGP is from flowering to maturity (Pingya and Biying, 1985; Xiuping, 2014). A total of 14 meteorological stations in the Songliao Plain were selected as the research stations. The meteorological data used in the present study was taken from the National Meteorological Information Center (http://www.resdc.cn/). Maize yield data were obtained from the China Planting Information Network (http://zzys.agri.gov.cn/), provincial statistical yearbooks, and the Jilin Meteorological Bureau, covering 30 years of data from 1985 to 2015. The standard geographical information data came from the National Catalogue Service for Geographic Information website (http://www.webmap.cn). The Supplementary Material can be accessed for more detailed data sources. In the present study, the inverse distance weighting method in ArcGIS software was used to interpolate and classify the statistical data of each site and obtain the corresponding spatial distribution map.

3. Methods

3.1. Indices

3.1.1. Crop water surplus and deficit index (CWSDI)

The CWSDI plays an essential role in formulating irrigation strategies and regional water resource allocation. In the present study, the CWSDI was constructed using ET_c and P_{ei} to reflect the water demand and water supply of maize at different growth stages (Eq. (1)) (Wang et al., 2018b):

$$CWSDI_i = \frac{P_{ei} - ET_{ci}}{ET_{ci}} \quad (1)$$

where, P_{ei} is the total effective rainfall in the ith growth stage (mm) (Eq. (2)); $CWSDI_i > 0$ indicates water surplus; $CWSDI_i < 0$ indicates water deficit; and $CWSDI_i = 0$ indicates balance of the water budget. Crop P_{ei} is

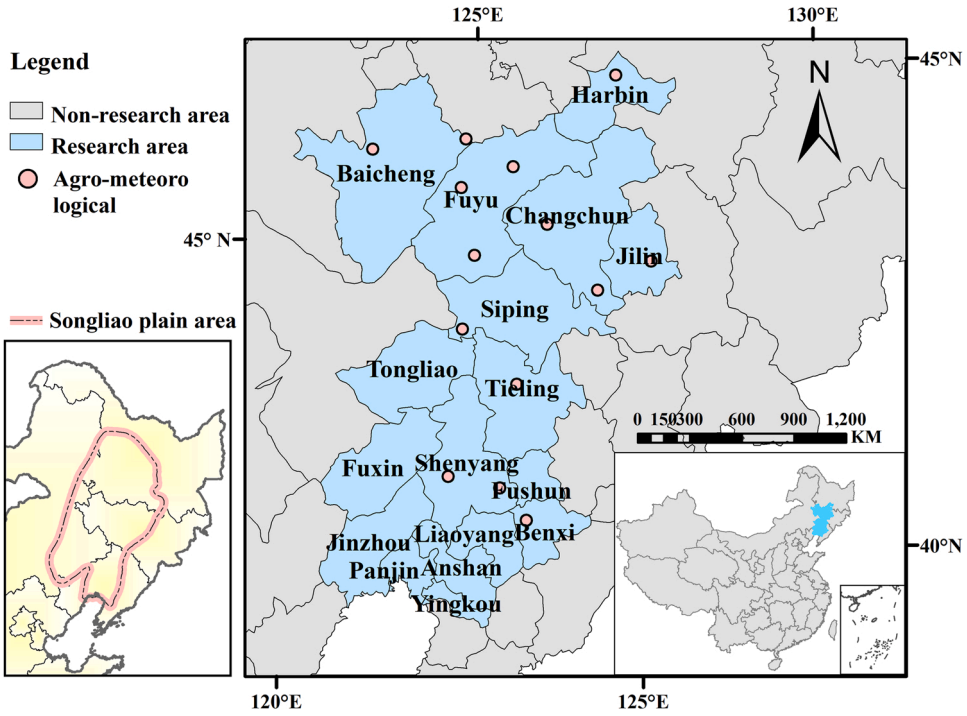

Fig. 1. Sketch map of the study area.

the portion of rainfall falling during the crop growing season that can be retained in the root zone for long enough to meet crop evapotranspiration requirements. It was calculated as follows:

$$P_{ei} = \sum_{j=1}^{n} P_{ej} \tag{2}$$

$$P_{ej} = \alpha_j \times P_j \tag{3}$$

Where, P_j is the total rainfall on the jth day (mm); P_{ej} is the effective rainfall amount on the jth day (mm); α is the effective utilization coefficient, $P_j \leq 5$ mm, $\alpha_j = 0$; $5 \leq P_j \leq 50$ mm, $\alpha_j = 0.9$; $P_j > 50$ mm, $\alpha_j = 0.75$. (Yang et al., 2021).

ET_{ci} is the water requirement of maize during the growing season, calculated using the simulation evapotranspiration of applied water model, which was developed based on the Penman–Monteith method proposed by the Food and Agriculture Organization (FAO) of the United Nations (Allen et al., 1998). The crop water demand was calculated daily (Eqs. (4)–(5)), which has been widely used in the calculation of water demand of maize (Yang et al., 2012, 2013):

$$ET_C = K_C \times ET_O \tag{4}$$

$$ET_O = \frac{0.408\Delta\left(R_n - G\right) + \gamma\frac{900}{T_{mean}+273}u_2\left(e_s - e_a\right)}{\Delta + \gamma(1 + 0.34u_2)} \tag{5}$$

where, ET_O is the potential evapotranspiration (mm d^{-1}); G is the soil heat flux density (MJ m^{-2} d^{-1}); γ is the wet and dry constant (kPa ℃$^{-1}$); and T_{mean} is the average temperature (℃). T_{mean} is defined as the average of the daily maximum temperature (T_{max}) and daily minimum temperature (T_{min}) within 24 h; R_n is the net radiation (MJ m^{-2} d^{-1}); e_s is the saturated water vapor pressure (kPa); e_a is the actual water vapor pressure (kPa); Δ is the slope of the saturated vapor pressure curve (kPa/℃); u_2 is 2 m high wind speed (m/s); and K_C is the crop coefficient of maize in a certain period (Paredes et al., 2020; Zhong et al., 2019). A more detailed calculation process of the indicators in the formula can be found on the FAO official website (http://chm.pops.int/Partners/FAO/tabid/293/Default.aspx).

The drought and flood grade standard levels of crop water surplus and the deficit index of maize were determined based on the drought grade of water deficit index specified in the drought intensity standard of spring maize in North China (China Meteorological Administration, 2015) and historical disaster data of typical representative stations in the study area (Table 1).

3.1.2. Heat stress index

The present study selected two heat stress indicators: HSI and EDD to characterize the occurrence and influence of heat stress during different growth stages of maize (Guo et al., 2019; Wang et al., 2018a; Zhang et al., 2017).

For every growth stage, HIS (°C) is the total days when $T_{max} \geq T_h$. EDD (°C d) is the total extreme growing degree-days, and it is calculated using Eqs. (6) and (7).

$$EDD = \sum_{d=1}^{N} ED_d \tag{6}$$

$$ED_d = \begin{cases} 0 & T_{max,d} < T_h \\ T_{max,d} - T_h & T_{max,d} \geq T_h \end{cases} \tag{7}$$

EDD is the cumulative degree of high temperature during a certain growth stage of maize. ED_i is the daily temperature greater than the heat

Table 1
Drought grade indexes of maize based on CWSDI.

Drought Grade	Vegetative Growth Period (VGP)	Vegetative and Reproductive Period (VRP)	Reproductive Growth Period (RGP)
Light Drought	-65 < CWSDI≤ −45	-50 < CWSDI≤ −35	-60 < CWSDI≤ −35
Middle Drought	-75 < CWSDI≤ −65	-60 < CWSDI≤ −50	-70 < CWSDI≤ −60
Heavy Drought	≤ −75	≤ −60	≤ −70

CWSDI represented for crop water surplus and deficit index

stress threshold, N is the total number of days in a certain growth stage of maize, $T_{max,\ d}$ represents the highest daily temperature, and T_h indicates the threshold temperature of heat stress in the maize-growing season. The values are shown in Table 2.

3.2. Historical effects of climate on maize growth

The Mann–Kendall (M–K) mutation test is widely used to test the trends of time series data of precipitation, air temperature, and water quality (Congbin and Qiang, 1992; Djaman et al., 2019). MATLAB 2016b software was used in the present study to perform the test. The M–K method can identify the mutation period and region based on the output of two sequences (UF and UB). For a time series x with n samples, an order sequence was constructed as:

$$s_k = \sum_{i=1}^{k} r_i, \qquad r_i = \begin{cases} 1, & xi > xj \quad j = 1, 2, \ldots, i \\ 0, & else \end{cases} \tag{8}$$

where the order column s_k is the cumulative number of values at time i greater than the number of values at time j, when $k = 1$, $s_1 = 0$.

Under the assumption that the time series were random and independent, the statistics were defined as:

$$UF_k = \frac{s_k - E(s_k)}{\sqrt{Var(s_k)}}, \quad k = 1, 2, \ldots, n \tag{9}$$

where $UF_1 = 0$, $E(s_k)$, $Var(s_k)$ are the mean and variance of cumulative number s_k, and when x_1, x_2, …, x_n are independent of each other and have the same continuous distribution.

$$E(s_k) = \frac{n(n-1)}{4} \tag{10}$$

$$Var(s_k) = \frac{n(n-1)(2n+5)}{72} \tag{11}$$

UF is a standard normal distribution, which is a statistical sequence calculated based on the time series x sequence x_1, x_2, …, x_n. According to the time sequence x, x_n, x_{n-1},., x_1, the above process is repeated to construct the inverse sequence UB.

3.3. Precondition cloud generator algorithm

Representing uncertain phenomena has always been the focus of natural science research. Among the uncertainties, randomness and fuzziness are the most critical (Chengguo et al., 2018; Mingyuan et al., 2016; Zheng-Jie et al., 2014). The cloud model uses three numerical characterizations of expectation (Ex), entropy (En), and super entropy (He) to associate fuzziness and randomness to form a map between qualitative and quantitative data (Dey and Changyu, 2004). Ex is the point in the universe space that can best represent the qualitative concept C. En reflects the uncertainty of qualitative concept C, and the range of the number domain that can be accepted by the linguistic value in the number domain, namely ambiguity. He is the dispersion degree of entropy, namely the entropy of entropy, and reflects the cohesion of each numerical value representing the linguistic value certainty, and the condensation degree of cloud droplets (Fig. 2).

After constructing the evaluation cloud, He was determined by experience based on the uncertainty and randomness of specific indicators, and subjective factors were strong, which weakened the randomness of the cloud model. Therefore, when building the composite disaster assessment cloud, based on the principle of assessment grade division, we used the reverse cloud generator to determine the He value in the assessment cloud, making the assessment cloud more objective (Tursken, 2006). Simultaneously, the multi-attribute evaluation method was used to calculate the influence grade of drought and heat on maize growth and development. The specific algorithm was obtained through the following steps:

Step 1: Calculation of the expectation and entropy of CWSDI and EDD.
Step 2: Utilization of an inverse cloud generator to determine He. Obtain eigenvalues $C_0 = [CG_C (Ex_C, En_C, He_C), CG_H (Ex_H, En_H, He_H)]$
Step 3: Generation of two normally distributed random numbers En_C' and En_H', satisfying $En_C' \in N (En_C, He_C)$ and $En_H' \in N(En_H, He_H)$, respectively.
Step 4: Calculation of the certainty μ, repeated until N cloud droplets are generated.

$$\mu_0 = \exp\left\{ -\left[\frac{(C_0 - Ex_C)^2}{2(En_C')^2} + \frac{(H_0 - Ex_H)^2}{2(En_H')^2} \right] \right\} \tag{12}$$

Step 5: Utilization of a precondition cloud generator algorithm. Given a sample $X_0 = [C_0, H_0]$. By inputting their corresponding concept cloud models, a group of membership degrees is obtained. The maximum value is retrieved and recorded as μ_{CH}.
Step 6: Construction of an evaluation cloud ($C(Ex_C, En_C, He_C, Ex_H, En_H, He_H)$) and an attribute cloud ($C^* (Ex^*_C, En^*_C, He^*C_C, Ex^*_H, En^*_H, He^*_H)$) according to the final certainty.

$$\begin{cases} Ex^* = Ex \times \mu_{CH} \\ En^* = En \times \mu_{CH} \\ He^* = He \times \mu_{CH} \end{cases} \tag{13}$$

Step 7: According to the description of the correlation degree, and the evaluation cloud and attribute cloud calculated in Step 6, k, representing the similarity of C* to C, is calculated by the eigenvalues of each level using formula 14. The influence level of composite events is determined by the maximum value of k (Guo et al., 2010, 2018; Zhang et al., 2014).

$$\begin{cases} k = \sum_{i=1}^{n} \frac{|N|}{|M|} \\ N = \{(Exi - 3Eni, Exi + 3Eni)\} \cap \{(Ex^*i - 3En^*i, Ex^*i + 3En^*i)\} \\ M = \{(Exi - 3Eni, Exi + 3Eni)\} \cup \{(Ex^*i - 3En^*i, Ex^*i + 3En^*i)\} \end{cases} \tag{14}$$

Table 2
Thresholds of heat stress indices during VGP, VRP, and RGP.

Period	Temperature threshold (℃)	Physiological basal temperature (℃)
Vegetative Growth Period (VGP)	≥ 33 (Jianyong, 2012)	10
Vegetative and Reproductive Period (VRP)	≥ 33 (Huang et al., 2016)	10
Reproductive Growth Period (RGP)	≥ 30 (Xiaogang et al., 2015)	10

RGP represented for reproductive growth period; VRP represented for vegetative and reproductive period; VGP represented for vegetative growth period.

3.4. Copulas

The copula function is a multidimensional joint distribution function defined in a [0,1] uniform distribution, which can be constructed by marginal distribution and correlation structure to describe the dependence among variables. Its theory can be expressed as follows: Let X and Y be continuous random variables, and their marginal distribution functions are FX(x) and FY(y), respectively, and the joint distribution function is F(x, y) (Salvadori and De Michele, 2004, 2010). If each marginal distribution function is continuous, there is a unique copula

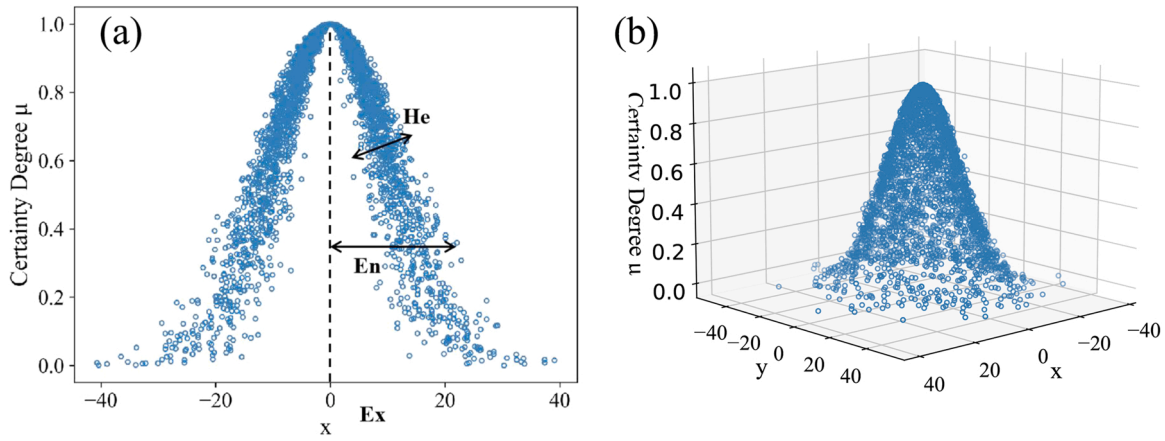

Fig. 2. Cloud model. (a) Cloud map of qualitative concept C (0, 10, 1). (b) Two-dimensional cloud map of qualitative concept C (0, 10, 1, 3, 15, 0.5).

function C (u, v), which makes:

$$F(x,y) = C[F_X(x), F_Y(y)] = C\ (u,v) \tag{15}$$

where, F(x, y) is the joint distribution function; C represents the copula function; u is the marginal distribution function of random variable X; and V is the marginal distribution function of random variable Y.

To construct the copula, we first measured the correlation between elements, and then determined the marginal distribution function of variables, and finally fitted and tested the copula. In the present study, the Spearman coefficient was used to measure the correlation of the variables to be extracted. For the marginal fitting, 17 common distribution functions were selected (Table SI. 1). Markov chain Monte Carlo simulation was used to calculate the parameters included in the copula function under the Bayesian framework (Sadegh et al., 2017, 2018). The goodness of fit (GOF) of the copula function was tested based on the root mean squared error (RMSE), Akaike information criterion (AIC), and Bayesian information criterion (BIC) between the theoretical distribution function and the empirical distribution function (Wang et al., 2020). The optimal copula function was established based on the principle that the smaller the RMSE, AIC, and BIC values were, the higher the GOF of the copula function was (Goodarzi et al., 2020; Sillmann et al., 2013):

$$RMSE = \sqrt{\frac{1}{n}\sum_{i=1}^{n}(pe_i - p_i)^2} \tag{16}$$

$$MSE = \frac{1}{n}\sum_{i=1}^{n}(pe_i - p_i)^2 \tag{17}$$

$$AIC = n\ln(MSE) + 2m \tag{18}$$

$$BIC = n\ln(MSE) + m\ln n \tag{19}$$

where, P_{ei} represents the empirical probability, p_i represents the theoretical probability, m is the number of model parameters, and n is the number of samples.

The marginal distribution function of X and Y and the calculation method of the MATLAB environment univariate return period were as follows:

$$F_X(x) = P(X \le x) = u \tag{20}$$

$$F_Y(y) = P(Y \le y) = v \tag{21}$$

$$T(x) = \frac{N}{n[1 - F_X(x)]} \tag{22}$$

$$T(y) = \frac{N}{n[1 - F_Y(y)]} \tag{23}$$

where N is the observation length of the sample and n is the number of times that a given value is exceeded in a specific period.

The formula of conditional probability and joint return period of joint events was as follows (Bai et al., 2020):

$$P(y_1 < Y < y_2 | x_1 < X < x_2) = \frac{P(x_1 < X < x_2, y_1 < Y < y_2)}{P(x_1 < X < x_2)} = \frac{C(u_2, v_2) - C(u_1, v_2) - C(u_2, v_1) + C(u_1, v_1)}{(u_2 - u_1)} \tag{24}$$

$$T\left(x,y\right) = \frac{N}{n[1 - C(u,v)]} \tag{25}$$

The corresponding code was written and calculated in MATLAB based on the relationship between X and Y.

4. Results

4.1. Temporal and spatial variation of drought and heat

4.1.1. Temporal and spatial variation of drought

Our analysis revealed the changing roles of P_{ei}, ET_c, and CWSDI during different growth stages of spring maize in the study area (Fig. 3). P_{ei} and CWSDI had similar trends. During the VGP (Fig. 3a), 2012 was the mutation year in the CWSDI. After 2012, the CWSDI changed from being stable to increasing. P_{ei} increased after 2012 and broke through the reliability line of + 1.98 of the M–K mutation test in 2015, exhibiting a distinct upward trend. The average value of Pei was 134.77 mm in 2011–2016, and 98.95 mm in 2006–2010. The average value of ET_c in 2011–2016 was 139.43 mm. In 1982 and 2004, there were extremely low points, with P_{ei} < 50 mm and CWSDI < −75%, belonging to extreme drought years. During the VRP (Fig. 3b), the CWSDI in 1997, 2000, 2014, and 2015 was lower than − 65%. The mutation points of CWSDI occurred in 1997 and 2008. Before 1997, CWSDI displayed a downward trend. Additionally, the mutations of P_{ei} and ET_c occurred around 1997. In 1996–2000, P_{ei} was 83.25 mm and ET_c was 132.20 mm. During 1991–1995, the average P_{ei} and ET_c were 114.84 and 118.17 mm, respectively. The average P_{ei} in 2001–2005 and 2006–2010 were 89.77 and 96.46 mm, respectively, and the average ET_c were 126.74 and 121.92 mm. After 2008, it showed a significant downward trend again. The P_{ei} in 2016 was only 68.04 mm. During the RGP (Fig. 3c), the mutation of CWSDI occurred in 1999. The average values of P_{ei} and ET_c before 1999 were 153.86 and 192.13 mm, respectively, whereas after 1999, these values were 129 and 196.71 mm,

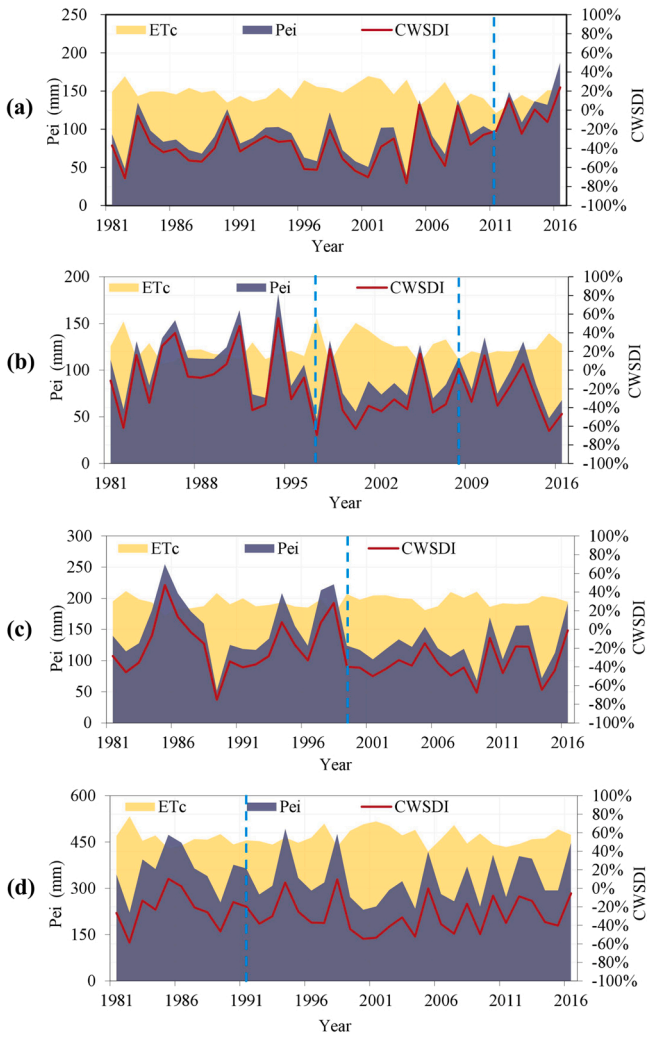

Fig. 3. Time series of maize P_{ei}, ET_c, and CWSDI at different growth stages of (a) VGP, (b) VRP, (c) RGP and (d) WGP from 1981 to 2016. The blue dotted line is the mutation year of CWSDI calculated using the M–K mutation test. RGP represented for reproductive growth period; VRP represented for vegetative and reproductive period; VGP represented for vegetative growth period; WGP represented for whole growth period; P_{ei} represented for effective rainfall; ET_c represented for crop water requirement. (For interpretation of the references to colour in this figure legend, the reader is referred to the web version of this article.)

respectively. The mean value of CWSDI decreased from − 0.19 to − 0.34. During the WGP (Fig. 3d), the overall trend of P_{ei} and ET_c was similar to that in RGP. The mutation period occurred around 1992. P_{ei} fluctuated significantly and the study area was in water deficit. Except for the VGP, the yield of maize in the study area might be reduced due to insufficient irrigation.

The annual P_{ei}, ET_c, and CWSDI of the three growth periods (VGP, VRP, and RGP) were calculated, and their multi-year average values were measured. The inverse distance weighting method was used for spatial interpolation and the distribution of water resources in the study area was analyzed (Fig. 4). The ranges of ET_c, P_{ei}, and CWSDI were 81–222 mm, 41–205 mm, and − 55–1%, respectively. There were pronounced differences during each growth period. In the VGP, the ET_c was 128–175 mm (Fig. 4a1). Except for Yingkou, the P_{ei} in most areas was between 68 and 123 mm, and the CWSDI changed significantly in the entire region, gradually decreasing from the north to south except in Harbin and Baicheng. The CWSDI in most areas ranged from − 46% to − 28% (Fig. 4c1). In the VGP, the water supply was deficient in most years. In the VRP, the ET_c in most areas ranged from 100 to 152 mm (Fig. 4a2). However, the ET_c in Shuangliao was 199 mm. P_{ei} was concentrated between 68 and 123 mm (Fig. 4b2). The demand for water by crops began to increase. The CWSDI ranged between − 28% and − 8%, and the drought in the entire region was light (Fig. 4c2). In RGP, the ET_c ranged from 175 to 222 mm (Fig. 4a3), and P_{ei} showed an increasing trend from northwest to southeast (Fig. 4b3). The P_{ei} in northwest China was 68–123 mm, whereas that in southeast China was 150–205 mm. Additionally, the CWSDI during this period showed an increasing trend from the northwest to the southeast (Fig. 4c3). The drought in Baicheng, Da'an, Qianan, Changling, and Shuangyang was particularly severe. In most years, precipitation was insufficient and evaporation was large.

4.1.2. *Temporal and spatial variation of heat*

The change laws of EDD and HSI during each growth period of maize in 35 y were calculated in the present study by simultaneously calculating the average maximum temperature (Fig. 5). The heat stress in the high latitudes (north) was more severe than that in the low latitudes (south) during the VGP and VRP (Fig. 5a). In the RGP, there was a trend of severe heat stress (Fig. 5a3), and Baicheng, Da'an, and Qianguo showed a high temperature trend (Fig. 5b3). Although the northern region was generally colder (Xiaoqing et al., 2015), HSI in the northern region was more severe than that in the southern region during the VGP and VRP. The growth period was delayed in the northern areas, especially the jointing and mature stages (Fig. SI. 1). The growth period in the northern region was delayed more severely, leading to maize being exposed to more heat than other regions. In the VGP and VRP, the maximum HSI in high-latitude areas (northwest) was above 34 °C. In the VGP, the average EDD in northwest China was 7.8 °C d, which was twice as high as that in the low latitudes (southeast) (Fig. 5a1). In the VRP, the average EDD in northwest China was 6.5 °C d (Fig. 5a2). In RGP, HSI was above 32 ℃ (Fig. 5b3), and EDD was 18 °C d (Fig. 5a3). The spatial variation of the mean value of the heat stress index was small. Over the last 35 years, the high-latitude areas (northwest) in Songliao Plain have been under severe heat stress during VGP and VRP. The maximum value of HSI ranged between 33.5 °C and 34.5 °C, and the maximum value of EDD was 38.2 °C d. In the RGP, the heat stress in low latitude areas (southeast) was severe. The maximum value of HSI ranged between 33.0 °C and 34.0 °C, and the maximum value of EDD was 75.4 °C d.

During the RGP, HSI showed a slight upward trend after 2010. During the VGP, HSI showed an apparent upward trend after 1990, and exceeded the reliability line of + 1.98 in 2002–2005, 2011, and 2014, reaching a significant level. During the VRP, HSI showed a significant downward trend from 1981 to 1997, fell below the reliability line of − 1.98 in 1990, and then showed an increasing trend. Simultaneously, the annual average maximum temperature in the Fig. 5c2 is similar to the trend of HSI. The average temperature is often higher after a sudden change year, with this phenomenon requiring further study.

4.2. *Uncertainty analysis of concurrent drought-heat events*

First, we corrected the data, chose a constant, multiplied it by CWSDI, called it relative CWSDI, and then fitted it to the cloud model (positive integer 1 was chosen as constant.). During 1981–2016, CWSDI ≤ 0.55 in the VGP and CWSDI ≤ 0.65 in the VRP and when the maximum temperature ≥ 33 ℃, then drought and extreme heat events occurred together. During the RGP and WGP periods, CWSDI ≤ 0.65 and when the highest temperature ≥ 30 ℃, drought and extreme heat events occurred together. Additionally, the EDD was graded by percentile, where $N^*(EDD_{max}–EDD_{min})$ for extremely high temperatures of different degrees. N was 10%, 30%, and 80%.

The drought grade standard of the CWSDI of maize was determined based on the drought grade of the water deficit index specified in the drought grade standard of spring maize in North China (China Meteorological Administration, 2015) and historical disaster data of typical

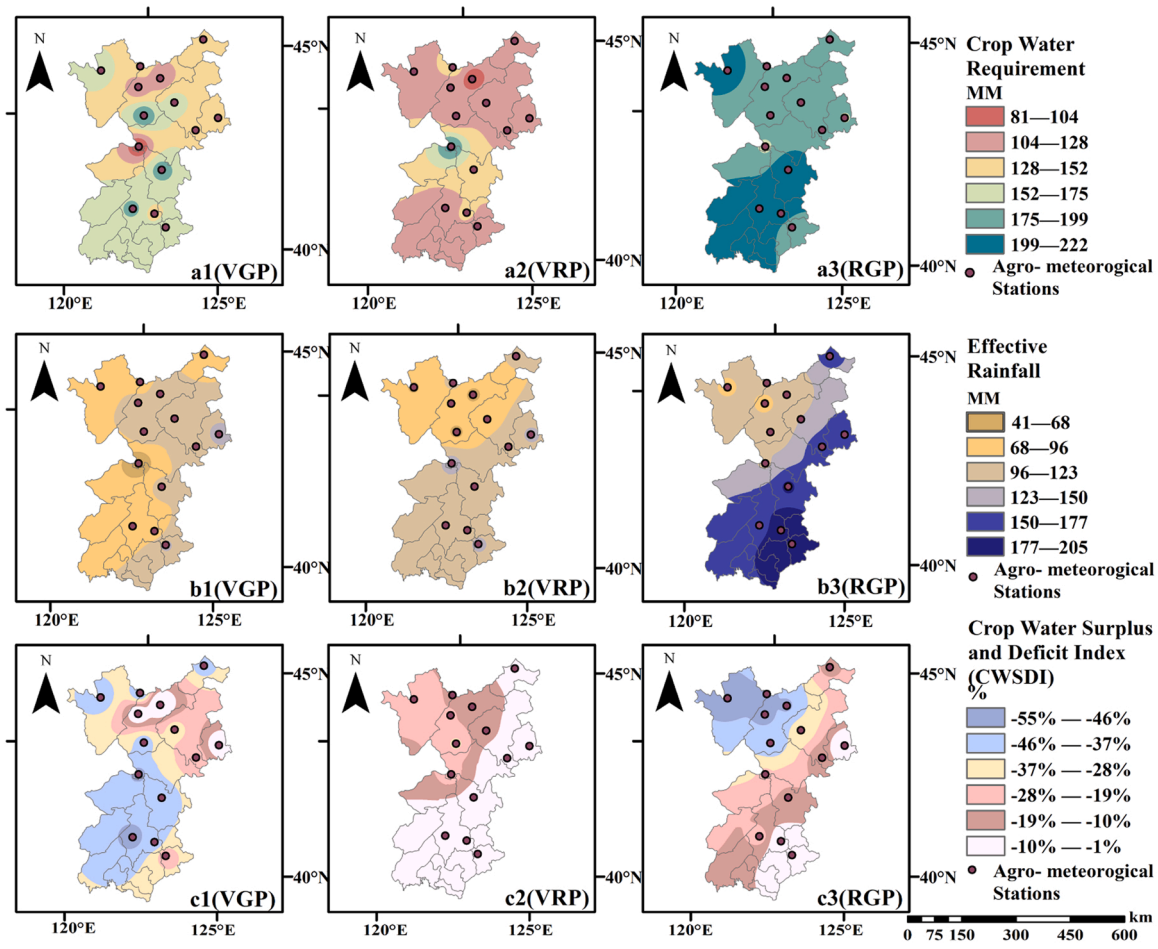

Fig. 4. Spatial distribution of the variation of effective rainfall (P_{ei}), crop water requirement (ET_c), and crop water surplus and deficit index (CWSDI) during growth stages for maize in the Songliao Plain. RGP represented for reproductive growth period; VRP represented for vegetative and reproductive period; VGP represented for vegetative growth period; WGP represented for whole growth period.

representative stations in the study area. Composite events were divided into three levels according to CWSDI and EDD levels. Three cloud characteristic values (Table 3) and conceptual cloud models (Fig. SI. 2) of each drought disaster risk grade were obtained from the interval threshold.

The similarity (k) of C* to C was calculated using the cloud algorithm, and the maximum value was retrieved. The evaluation result corresponding to the maximum value was the impact degree of the corresponding concurrent events on crops. From 1981 to 2016, in the VGP, there were five events above level III in Baicheng, Da'an, Shuangliao, and Xinmin. In the VRP, Baicheng, Da'an, Qianan, Qianguo, Changtu, and Xinmin had more than five level III events and more than 10 level II events. More than 10 level III events occurred in Changling and Nong'an. In the RGP, Baicheng, Da'an, Qianan, Qianguo, Changling, Nong'an, and Shuangliao had more than five level III events.

The period was divided into three intervals: 1981–1992, 1993–2004, and 2005–2016. The frequencies of concurrent events in different degrees during the three periods were calculated (Fig. 6). The frequency of level I concurrent events was higher in VGP and RGP. Level II events occurred more frequently in VRP. Harbin, Shuangliao, and Benxi were the regions where level I events in the VGP showed an apparent and continuous increasing trend during all three periods. In the VGP, level I events showed an apparent and continuous decreasing trend in Changling, whereas in the RGP, it was only found in Baicheng. In the VRP, level II concurrent events showed an apparent and continuous increasing trend in Benxi, whereas a decreasing trend was seen in Qianan, Changling, Shuangliao, Xinmin, and Shenyang, and occurrence probability of level III events in Qianan, Changling, and Xinmin continued to increase.

4.3. Probability analysis of concurrent drought-heat events

The copula function was used to establish the joint distribution probability and recurrence period, which can reflect the risk of joint events to evaluate the occurrence regularity of drought and heat during the growth period of spring maize.

4.3.1. Construction of marginal distribution function

To construct the copula joint distribution function effectively, the appropriate marginal distribution function of CWSDI and EDD was determined. During the VRP and RGP, both drought and heat have a high occurrence probability, with heat having the most significant impact on maize yield (Gao et al., 2012). Therefore, the present study performed a bivariate analysis of the VRP and RGP of maize at 14 stations. A total of 17 marginal distribution functions were used to fit CWSDI and EDD, and AIC and RMSE were selected to determine the optimal marginal distribution function. The Chi-square test was used to estimate the parameters of the marginal distribution function, and the Kolmogorov–Smirnov method was used to evaluate the GOF. All optimal distributions passed the $\alpha = 0.05$ significance test (Tables SI. 3 and SI. 4). GPD, GEV, Normal, Logistic, and EVD were used in the present study (Table SI. 2). Before establishing the joint distribution function, we used the Kendall rank correlation coefficient (τ) and Spearman rank correlation coefficient (ρ) to test the correlation between CWSDI and EDD. In

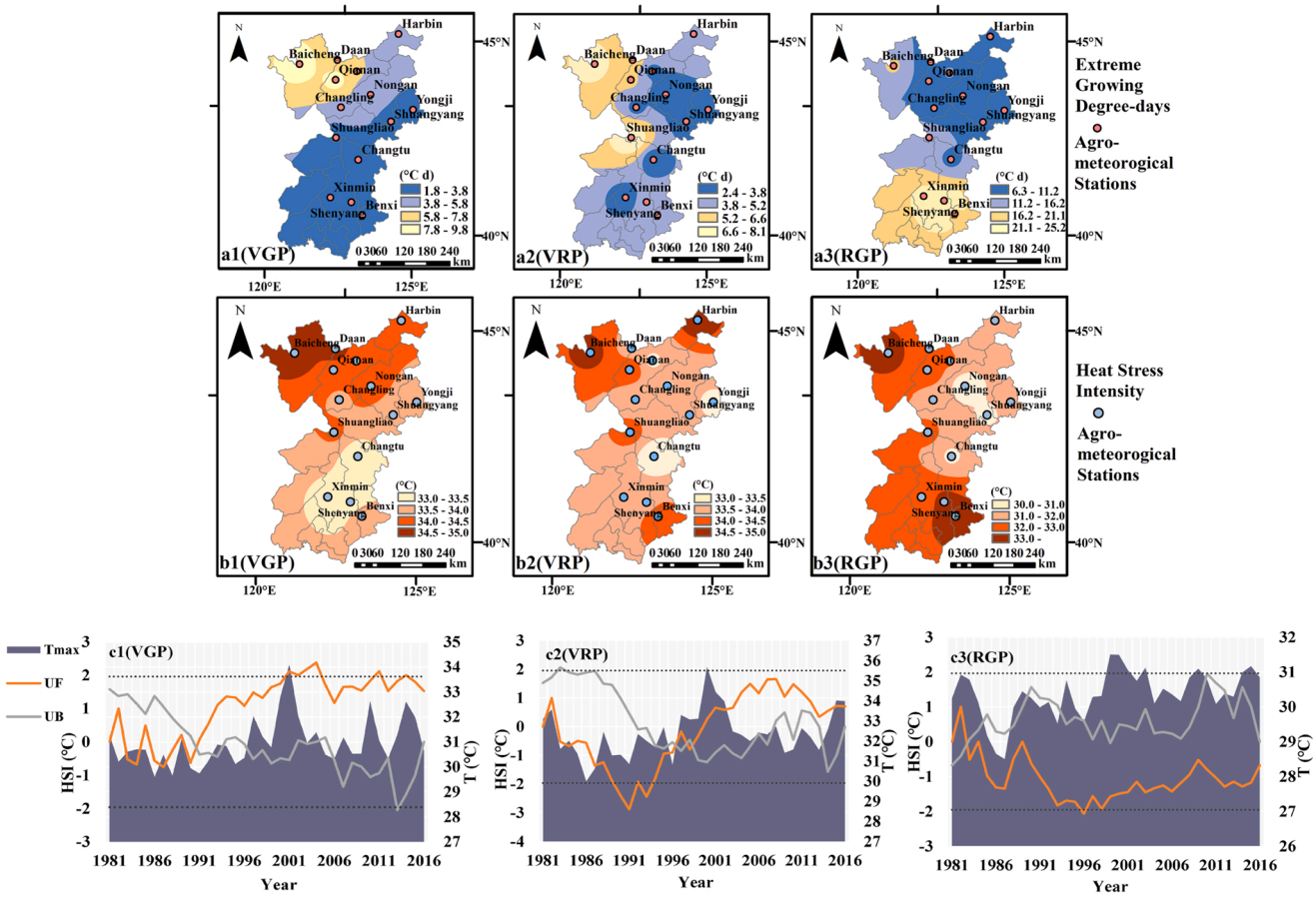

Fig. 5. Temporal and spatial distribution of HSI, EDD, and average maximum temperature (Tmax) during the maize growth period. (a) Series a (a1, a2, and a3) shows the spatial distribution characteristics of EDD in different growth stages (VGP, VRP, and RGP) of maize in the study area. (b) Series b (b1, b2, and b3) shows the spatial distribution characteristics of HSI in different growth stages (VGP, VRP, and RGP) of maize in the study area. (c) Series c (c1, c2, and c3) shows the variations of the M–K test of HSI and EDD during the growth stages for maize. The blue part indicates the average maximum temperature of each growth period in the study area every year. The upper and lower black dotted lines indicate the 0.05 significance of the M–K test. RGP represented for reproductive growth period; VRP represented for vegetative and reproductive period; VGP represented for vegetative growth period; EDD represented for Extreme growing degree-days; HSI represented for Heat stress intensity. (For interpretation of the references to colour in this figure legend, the reader is referred to the web version of this article.)

Table 3
Cloud characteristics of drought hazard level based on the CWSDI and EDD.

Period	Levels	CWSDI			EDD		
		Ex	En	He	Ex	En	He
VGP	I	0.45	0.09	0.03	7.64	3.24	0.45
	II	0.30	0.04	0.01	21.01	8.11	0.37
	III	0.13	0.11	0.02	34.38	3.24	0.33
VRP	I	0.58	0.06	0.02	7.02	2.98	0.79
	II	0.45	0.04	0.01	19.31	7.45	0.94
	III	0.20	0.17	0.03	31.59	2.98	0.72
RGP	I	0.53	0.11	0.03	15.08	6.40	0.78
	II	0.35	0.04	0.01	41.47	16.00	0.69
	III	0.15	0.13	0.03	67.86	6.40	0.63
WGP	I	0.45	0.08	0.03	16.92	7.18	0.84
	II	0.30	0.04	0.01	46.53	17.96	0.69
	III	0.13	0.11	0.02	76.14	7.18	0.35

Levels I, II, and III represented for the mild, moderate, and severe effects on maize growth, respectively. Ex represented for expectation; En represented for entropy; He represented for super entropy. CWSDI represented for crop water surplus and deficit index; EDD represented for extreme growing degree-days. RGP represented for reproductive growth period; VRP represented for vegetative and reproductive period; VGP represented for vegetative growth period; WGP represented for whole growth period.

VRP, the τ values were above 0.2 (maximum 0.49, Baicheng), and the ρ values were above 0.25 (maximum 0.69, Baicheng). The τ value in RGP was above 0.2, except in Qianguo (the maximum value was 0.44 in Songliao). ρ values were all above 0.2 (the maximum value was 0.53 in Baicheng). All correlation coefficients passed the significance tests of $\alpha = 0.01$, 0.05, and 0.2, indicating that a few sites had a strong correlation, most sites had medium intensity correlation, and some sites had a weak correlation.

4.3.2. *Probability analysis based on Copula function*

The construction of the copulas function is the premise to further understand the joint probability distribution. The method to preprocess the data in the present study was the same as that for the cloud model (You et al., 2018). Table 4 shows the optimal coupling function and its parameters for the VRP and RGP of maize at each station in the study area. We used the AIC, BIC, Nash–Sutcliffe efficiency (NSE), and RMSE to test the GOF. The GOF evaluation of the copula function met the standard. Therefore, the optimal copula functions of RGP were mainly Gaussian copula and Frank copula, whereas VRP was mainly Gaussian copula.

4.3.3. *Analysis of joint probability and return period based on copula function*

Based on the copula function at each station, the probability of heat and drought conditions and the co-occurrence return period were

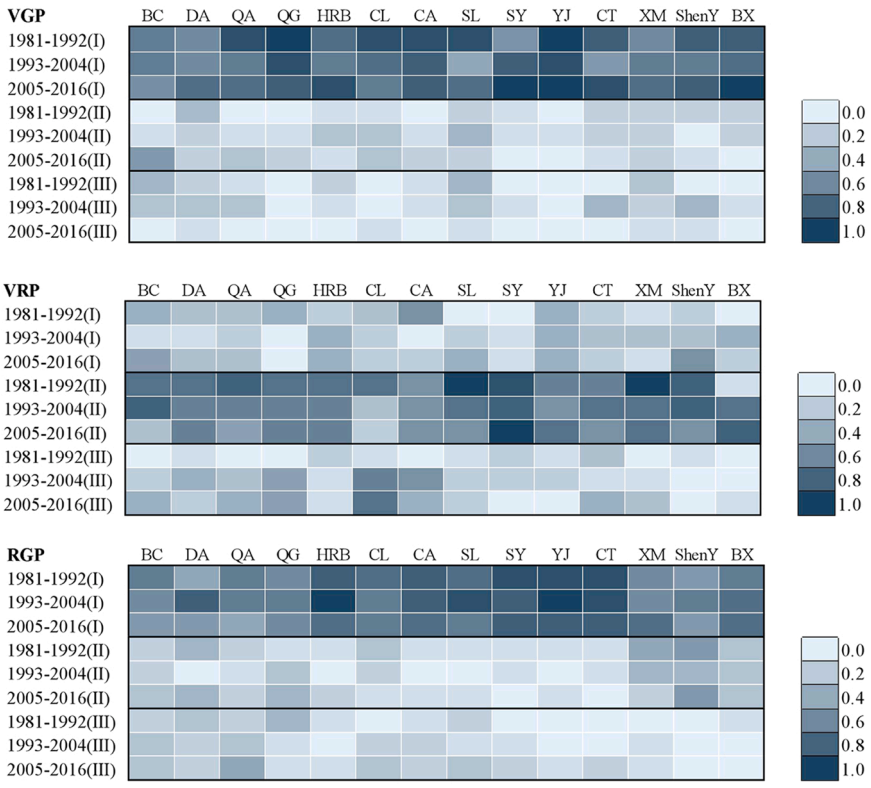

Fig. 6. Frequency of concurrent drought and heat events in 1981–1992, 1993–2004, and 2005–2016. RGP represented for reproductive growth period; VRP represented for vegetative and reproductive period; VGP represented for vegetative growth period. (BC: Baicheng; DA: Daan; QA: Qianan; QG: Qianguo; HRB: Harbin; CL: Changling; CA: Nongan; SL: Shuangliao; SY: Shuangyang; YJ: Yongji; CT: Changtu; XM: Xinmin; ShenY: Shenyang; BX: Benxi).

Table 4
Test of goodness of fit (GOF) of different copula functions.

Zone	Vegetative and Reproductive Period (VRP)					Reproductive Growth Period (RGP)				
	Copula functions	Parameter	AIC	RMSE	NSE	Copula functions	Parameter	AIC	RMSE	NSE
Baicheng	Gumbel	2.1114	-123.45	0.16	0.99	Gumbel	1.4454	-110.80	0.19	0.99
Daan	Gaussian	0.5127	-92.75	0.25	0.97	Frank	1.3076	-73.27	0.34	0.98
Qianan	Gaussian	0.4233	-100.66	0.23	0.98	Gaussian	0.2949	-113.74	0.19	0.99
Qianguo	Gaussian	0.3281	-96.31	0.24	0.97	Gaussian	0.2949	-105.31	0.21	0.98
Harbin	Gaussian	0.1396	95.66	0.24	0.97	Gaussian	0.2756	-76.65	0.32	0.95
Changling	Gaussian	0.1396	-101.49	0.22	0.98	Gaussian	0.4054	-76.65	0.25	0.97
Nongan	Gaussian	0.5254	-89.65	0.27	0.96	Gaussian	0.2853	-76.65	0.18	0.98
Shuangliao	Gaussian	0.7116	-93.08	0.25	0.97	Gaussian	0.2835	-76.65	0.25	0.96
Shuangyang	Gaussian	0.4784	-113.55	0.19	0.98	Frank	3.5038	-94.12	0.25	0.98
Yongji	Frank	2.4836	-107.31	0.20	0.98	Frank	1.838	-94.90	0.25	0.97
Changtu	Clayton	1.0742	-96.60	0.24	0.97	Gaussian	0.292	-86.93	0.28	0.97
Xinmin	Frank	3.3759	-128.50	0.15	0.99	Frank	1.226	-88.19	0.27	0.97
Shenyang	Frank	3.6431	-128.77	0.15	0.99	Frank	2.4163	-82.63	0.29	0.97
Benxi	Gumbel	1.5618	-102.45	0.22	0.98	Gumbel	1.7843	-110.52	0.20	0.99
Songliao	Clayton	1.9049	-94.71	0.25	0.97	Frank	1.5346	-77.26	0.32	0.96

RMSE represented for root mean squared error; AIC represented for Akaike information criterion; BIC represented for Bayesian information criterion.

calculated. Probability and co-occurrence return periods are representative of concurrent event risk. A shorter co-occurrence return period represents a higher risk. Using these, we could describe the risk of concurrent events. The degree of certainty of each sample point and the influence level of composite events were calculated using the two-dimensional precondition cloud generator algorithm. The grouping of the influence degree of concurrent events for maize was consistent with the grouping constructed using the cloud model.

In the VRP, the average occurrence probability of mild (I), moderate (II), and severe (III) concurrent events was 21.9%, 1.7%, and 0.35%, respectively (Fig. 7). The conditional probability of moderate drought-heat events decreased from the northwest to the southeast, and the maximum value appeared around Baicheng, reaching 50% (Fig. 7a1). There was a 1–4 y periodical oscillation, which occurred frequently. Harbin, Shuangyang, Yongji had a long return period of more than three years (Fig. 7b1). The occurrence probability of severe events was small, and the presentation range was similar to that of moderate events (Fig. 7a2). The return period in the south and northwest was 5–20 y, and the return period of more than 20 y covered an extensive range (Fig. 7b2). The joint occurrence probability of extremely severe events was extremely low, with a maximum probability of 1.12% (Fig. 7a3). The return period of concurrent events was longer in most areas of the entire study area, and was approximately 30–100 y in only a few surrounding areas (Fig. 7b3).

In the RGP, the average occurrence probability of I, II, and III concurrent events was 23.1%, 8.2%, and 0.12%, respectively, and the

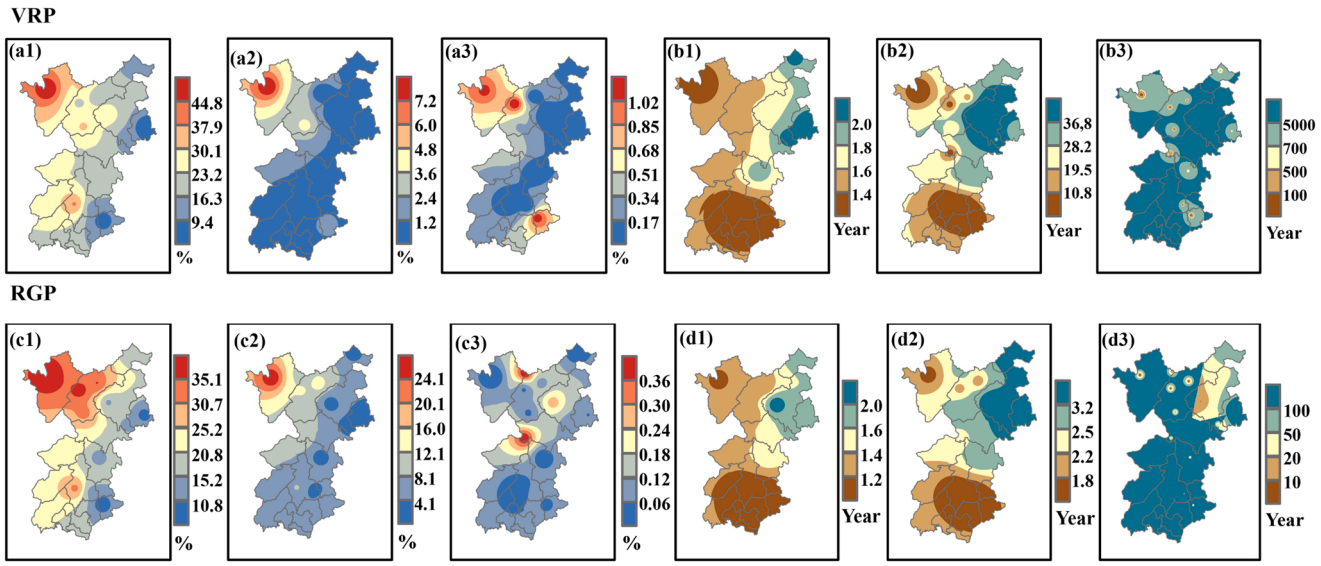

Fig. 7. Conditional probability(a1, a2, a3, c1, c2, c3) and spatial distribution(b1, b2, b3, d1, d2, d3) of the return period of drought-heat events in maize VRP and RGP stages in Songliao Plain. Mild(a1, b1, c1, d1), moderate(a2, b2, c2, d2), and severe(a3, b3, c3, d3) concurrent events represent the level I, level II, and level III concurrent events under the cloud model, respectively. RGP represented for reproductive growth period; VRP represented for vegetative and reproductive period.

maximum occurrence probability of moderate concurrent events was 50.7%, mainly concentrated in Baicheng and Da'an. Overall, the conditional probability of occurrence of concurrent events showed a downward trend from the west to the east (Fig. 7c1). The co-occurrence return period was concentrated in 1–3 y, occurring frequently (Fig. 7d1). The joint probability distribution of severe concurrent events was similar to that of moderate disasters; however, the probability of occurrence in most areas was lower than 16% (Fig. 7c2). The return period of co-occurrence increased from the south to the north, primarily from 1 to 2.5 y in the south and from 2 to 5 y in the north (Fig. 7d2). The occurrence of extremely severe disasters in the study area was an extremely low probability event (Fig. 7c3). The co-occurrence return period in the south was more than 100 y. The likelihood of extremely heavy concurrent events was low, and the return period in very few areas was approximately 20–50 y (Fig. 7d3). There was a warming trend in the study area; however, most had small warming ranges. From the time trend analysis, the probability of concurrent events of various degrees increased from 2011 to 2016.

5. Discussion

Previous studies on natural disasters have primarily focused on a single meteorological factor. The occurrence of a disaster may be the extreme state of a single variable; however, it is more likely to be the result of a combination of variables. It is necessary to know more about the non-stationarity of the climate system and the combination principle of climatic variables to understand the process and principle of complex disasters to recognize, quantify, and prevent risks.

Climate warming promotes drought formation and aggravates its severity (Cairns et al., 2013; Castro-Nava et al., 2014; Lipiec et al., 2013). Zhang et al. (2021) found that drought was the most common extreme weather event after 2000, and its influence was expanding, adversely affecting the growth and development of maize. Liu et al. (2013b) observed that high latitudes in the northern hemisphere were more susceptible to climate change by comparing the research results of many countries, and the northern boundary of maize planting in the northeast had extended northward. Additionally, the application of model simulation confirmed that the climate warming in northeast China has reached the level that will affect the growth of maize (Liu et al., 2013a). Thus, it is indisputable that crops are exposed to and affected by heat (Coumou et al., 2013; Yin et al., 2016b).

The results in the present study showed that P_{ei} distribution in the VGP was increasing. During the VRP and RGP, ET_c showed a downward trend, whereas the crop water demand increased. This trend appeared more frequently after 2000, especially during the RGP stage (Figs. 4 and 5). The P_{ei} of maize during different growth stages along the Songliao Plain showed a decreasing trend from the southeast to the northwest, with the northwest region expected to face more effects from frequent and severe droughts (Yin et al., 2016a; Zhang and Hu, 2018). During the VGP and VRP, HSI in the high latitudes was more severe than that in the low latitudes. In the RGP, EDD changed more, increasing from south to north (Fig. 6), which was contrary to the trend of P_{ei}. Heat affects rainfall and crop water demand to a certain extent and promotes drought. However, during other critical growth periods, only a few stations showed a significant warming trend, with apparent regional differences. Previous studies have confirmed the temperature increase in northeast China (Li et al., 2020b; Li and Amatus, 2020).

Guo et al. (2020) and Guna et al. (2019) used excess heat factors and SPEI to analyze climate change in China. Li et al. (2020a) analyzed the summer heat and drought in northeast China based on greenhouse emissions. Their results verified that the frequency of drought and heat would increase further from a future climate model. Our findings were similar to those of previous studies. According to the spatial and temporal law, most areas in the study area are in a state of worsening drought and increasing heat events. Drought events occurred more frequently in 2005–2016 than in 1981–1992 and 1993–2004. The characteristics of 2004, 2011, and 2014 included low P_{ei} and high temperature. This was the same as the typical drought year recorded in the disaster ceremony and disaster record provided by the China Meteorological Data Network. Additionally, Wang et al. (2018b) showed similar results. From the similarity of composite events calculated using the cloud model, most areas in the study area showed level III events during these years.

Previous study results have shown a phenomenon of high temperature in northeast China; however, the negative effect on yield can be eliminated by changing planting boundaries and plant varieties or increasing irrigation (Zhao et al., 2014; Siebert et al., 2017). Moreover, extreme temperatures will have varying influences across northeast China (Liu et al., 2012). Some researchers support that heating alone cannot have a critical negative effect on the growth of maize (Chen et al., 2011). The present study showed that the occurrence probability of moderate and higher concurrent events in the VRP and the RGP of plants

was higher in northwest China, which was consistent with the analysis results of the drought-heat events occurrence law. In the RGP, the return period of moderate and severe concurrent events was concentrated in 1–4 y, partly due to the low selected EDD range. This showed a gradual warming trend in the Pingyuan area of the Songliao Plain. In the correlation analysis between the relative meteorological output and the joint distribution probability, only some areas passed the significance test. Northeast China has not yet created a long-term and large-scale warming mode, which is generally concentrated on the slight increase and extension of the highest temperature and higher minimum temperature (Chen et al., 2011). Under water deficit conditions, the decrease in transpiration saves soil water, which might reduce the influence of heat (Manderscheid et al., 2015). Under the background of rain-fed irrigation, the principle that warming and drought simultaneously affect maize production (including but not limited to yield) needs to be further explored.

Several points in our study require attention. First, the results provide a reference for understanding the occurrence and regularity of drought disaster concurrent events. However, crops in northeast China may suffer from freezing and waterlogging, and from heat and drought. Due to climate change in the future, studying the effect of various extreme weather events on crop production is required. Second, the results provide a reference for the application of the cloud model and the copula function in agrometeorology and disaster risk assessment and management. This method can further reduce the influence of system uncertainty on the error of evaluation results and can be explored further in future research. However, the accuracy of the cloud and copula models mainly depends on the classification of the disaster grades and the determination of the cloud characteristics of each grade. The influence of precipitation and temperature on crops has a process of "atmosphere-soil-vegetation." Due to the differences in regional hydrology, meteorology, and underlying surface conditions, and the differences in temperature, canopy temperature, and underlying surface temperature, the selection of composite disaster indicators and the classification standard of concurrent disaster are controversial. The further application of the cloud and copula models should closely combine the disaster-causing mechanism, evolution law, and risk-causing mechanism of disasters on crops, and reveal the new characteristics of agrometeorological disasters under the background of climate change.

6. Conclusions

A probability assessment method of concurrent events during different growth stages of maize based on precipitation and temperature indexes was proposed. The main objective of the present study was to introduce the cloud model to identify the uncertainties in the evaluation of complex systems, and improve the objectivity and adaptability of the evaluation results. Then, combined with the copula model, the occurrence law of drought and high temperature combined disasters during different growth stages of maize was analyzed, and applied in the Songliao Plain. The application results were as follows:

(1) Warming during the VGP and VRP mainly occurred in high-latitude areas. In the RGP, the southern region had frequent high temperatures. Artificially delaying the growth period of maize makes it easier for maize to be exposed to high temperatures. Drought is still the main meteorological disaster affecting maize yield in the study area.
(2) The probability of the co-occurrence of drought and heat increased from the southeast to the northwest during the RGP stage, and the western region was more likely to be affected by moderate concurrent events. The Baicheng area was more likely to suffer from severe or greater concurrent events. Therefore, these areas need to formulate effective and feasible countermeasures to mitigate and prevent losses caused by drought and heat disasters.

In summary, the present study provides a meaningful reference for a better understanding of the occurrence laws of drought, heat, and concurrent events during crop growth periods, and how to optimize the agricultural management of maize. The present study also provides a basis for the future construction of multi-disaster risk dynamic assessment technology. Although the proposed model provides a useful tool for evaluating multiple joint behaviors, it fails to describe the complexity of drought and heat effects on crops. Comprehensive disaster hazard assessment depends on the construction of the assessment model and the disaster grade division. Therefore, it is imperative to analyze the disaster-causing mechanism, quantify the risk, and optimize the evaluation model under future climate change. Ways to apply this method to hazard assessment will be the focus of our future research.

Declaration of Competing Interest

The authors declare that they have no known competing financial interests or personal relationships that could have appeared to influence the work reported in this paper.

Acknowledgements

This study is supported by the National Key Research and Development Program of China (2019YFD1002201); The National Natural Science Foundation of China (41877520); The Science and Technology Development Planning of Jilin Province (20190303018SF); Key Research and Projects Development Planning of Jilin Province (20200403065SF); The Science and Technology Planning of Changchun (19SS007).

Appendix A. Supporting information

Supplementary data associated with this article can be found in the online version at doi:10.1016/j.agwat.2021.107238.

References

AghaKouchak, A., Cheng, L., Mazdiyasni, O., Farahmand, A., 2014. Global warming and changes in risk of concurrent climate extremes: Insights from the 2014 California drought. Geophys. Res. Lett. 41, 8847–8852. https://doi.org/10.1002/2014GL062308.

Allen, R.G., Pereira, L.S., Raes, D., Smith, M., 1998. Crop Evapotranspiration: guidelines for Computing Crop Water Requirements. Food and Agriculture Organization of the United Nations, Rome, Italy.

Bai, Y., Wang, Y., Chen, Y., Zhang, L., 2020. Probabilistic analysis of the controls on groundwater depth using Copula Functions. Hydrol. Res. 51, 406–422. https://doi.org/10.2166/nh.2020.147.

Bai, Z., 1998. The structure and dynamic change of the farmland in the Songliao Plain "Corn Belt. Acta Geogr. Sin. 53, 225–232 (in Chinese).

Cairns, J.E., Crossa, J., Zaidi, P.H., Grudloyma, P., Sanchez, C., Luis Araus, J., Thaitad, S., Makumbi, D., Magorokosho, C., Bänziger, M., Menkir, A., Hearne, S., Atlin, G.N., 2013. Identification of drought, heat, and combined drought and heat tolerant donors in maize. Crop Sci. 53, 1335–1346. https://doi.org/10.2135/cropsci2012.09.0545.

Castro-Nava, S., Ramos-Ortíz, V.H., Reyes-Méndez, C.A., Huerta, A.J., 2014. Grain yield, photosynthesis and water relations in two contrasting maize landraces as affected by high temperature alone or in combination with drought. Maydica 59, 104–111.

Chen, C., Lei, C., Deng, A., Qian, C., Hoogmoed, W., Zhang, W., 2011. Will higher minimum temperatures increase corn production in Northeast China? An analysis of historical data over 1965–2008. Agric. . Meteorol. 151, 1580–1588. https://doi.org/10.1016/j.agrformet.2011.06.013.

Chen, H., Sun, J., 2017. Anthropogenic warming has caused hot droughts more frequently in China. J. Hydrol. 544, 306–318. https://doi.org/10.1016/j.jhydrol.2016.11.044.

Chen, J., Zhao, S., Shao, Q., Wang, H., 2012. Risk assessment on drought disaster in China based on integrative cloud model. Res. J. Appl. Sci. Eng. Technol. 4, 1137–1146.

Chen, Y., Zhang, Z., Wang, P., Song, X., Wei, X., Tao, F., 2016. Identifying the impact of multi-hazards on crop yield-A case for heat stress and dry stress on winter wheat yield in northern China. Eur. J. Agron. 73, 55–63. https://doi.org/10.1016/j.eja.2015.10.009.

Chengguo, W., Lu, B., Xia, B., Juliang, J., Shangming, J., 2018. Risk assessment and division model for regional drought disaster based on cloud model and bootstrap method. J. Nat. Resour. 33, 684–695 (in Chinese).
China Meteorological Administration, 2015. The Drought Grades for Spring Maize in North. QX/T 259-2015. China Meteorological Press, Beijing,China (in Chinese).
Church, J., Clark, P., Cazenave, A., Gregory, J., Unnikrishnan, A., 2013. Climate Change 2013: The Physical Science Basis. Contribution of Working Group I to the Fifth Assessment Report of the Intergovernmental Panel on Climate Change. Cambridge University Press, United Kingdom and New York.
Congbin, F., Qiang, W., 1992. The deifniit on and deteetion of the abrupt cilmatic change. Chin. J. Atmos. Sci. 16, 482493 (in Chinese).
Coumou, D., Robinson, A., Rahmstorf, S., 2013. Global increase in record-breaking monthly-mean temperatures. Clim. Change 118, 771–782. https://doi.org/10.1007/s10584-012-0668-1.
Dao-Wei, Z., Zheng-Xiang, Z., Ying-Hua, J., Ping, W., 2010. Regionalization and distribution pattern of vegetation of Northeast China. Chin. J. Plant 34, 1359–1368.
Dey, L.I., Changyu, L., 2004. Study on the universality of the normal cloud model. Eng. Sci. 6, 28–34 (in Chinese).
Djaman, K., O'Neill, M., Diop, L., Bodian, A., Allen, S., Koudahe, K., Lombard, K., 2019. Evaluation of the Penman-Monteith and other 34 reference evapotranspiration equations under limited data in a semiarid dry climate. Theor. Appl. Climatol. 137, 729–743. https://doi.org/10.1007/s00704-018-2624-0.
Fang, W., Huang, S., Huang, G., Huang, Q., Wang, H., Wang, L., Zhang, Y., Li, P., Ma, L., 2019. Copulas-based risk analysis for inter-seasonal combinations of wet and dry conditions under a changing climate. Int. J. Climatol. 39, 2005–2021. https://doi.org/10.1002/joc.5929.
Gao, X., Wang, C., Zhang, J., Xue, X., 2012. Crop water requirement and temporal-spatial variation of drought and flood disaster during growth stages for maize in Northeast during past 50 years. Nongye Gongcheng Xuebao Trans. Chin. Soc. Agric. Eng. 28, 101–109. https://doi.org/10.3969/j.issn.1002-6819.2012.12.017.
Goodarzi, M.R., Fatehifar, A., Moradi, A., 2020. Predicting future flood frequency under climate change using copula function. Water Environ. J. 34, 710–727. https://doi.org/10.1111/wej.12572.
Guna, A., Zhang, J., Tong, S., Bao, Y., Han, A., Li, K., 2019. Effect of climate change on maize yield in the growing season: a case study of the Songliao Plain maize belt. Water 11, 2108. https://doi.org/10.3390/w11102108.
Guo, E., Wang, Y., Bao, Y., 2020. Assessing spatiotemporal variation of heat waves during 1961–2016 across mainland China. Int. J. Climatol. 40, 3036–3051. https://doi.org/10.1002/joc.6381.
Guo, J., Zhang, W., Zhao, Y., 2018. Method of multidimensional cloud model for rockburst prediction. Chin. J. Rock. Mech. Eng. 37, 1199–1206. https://doi.org/10.13722/j.cnki.jrme.2017.1522.
Guo, J., Jin, J., Tang, Y., Wu, X., 2019. Design of temperature insurance index and risk zonation for single-season rice in response to high-temperature and low-temperature damage: a case study of Jiangsu province, China. Int. J. Environ. Res. Public Health 16. https://doi.org/10.3390/ijerph16071187.
Guo, R., Xia, J., Dong, S., Long, M., 2010. Multiple attribute evaluation method based on multidimensional cloud mode. Comput. Sci. 37, 75–77 (in Chinese).
Huang, S., Huang, Q., Zhang, H., Chen, Y., Leng, G., 2016. Spatio-temporal changes in precipitation, temperature and their possibly changing relationship: a case study in the Wei River Basin, China. Int. J. Climatol. 36, 1160–1169. https://doi.org/10.1002/joc.4409.
Jianyong, M., 2012. Scenario Analysis of the Impact of High temperature and drought on corn yield in the Northeastern Chinese Marketplace. Chin. Acad. Agric. Sci. (in Chinese).
Killi, D., Bussotti, F., Raschi, A., Haworth, M., 2017. Adaptation to high temperature mitigates the impact of water deficit during combined heat and drought stress in C3 sunflower and C4 maize varieties with contrasting drought tolerance. Physiol. Plant. 159, 130–147. https://doi.org/10.1111/ppl.12490.
Leonard, M., Westra, S., Phatak, A., Lambert, M., van den Hurk, B., Mcinnes, K., Risbey, J., Schuster, S., Jakob, D., Stafford-Smith, M., 2014. A compound event framework for understanding extreme impacts. Wiley Interdiscip. Rev. Clim. Chang. 5, 113–128. https://doi.org/10.1002/wcc.252.
Li, H., Chen, H., Sun, B., Wang, H., Sun, J., 2020a. A detectable anthropogenic shift toward intensified summer hot drought events over Northeastern China. Earth Sp. Sci. 7 https://doi.org/10.1029/2019EA000836.
Li, C., Sun, Y., Zwiers, F., Wang, D., Zhang, X., Chen, G., Wu, H., 2020b. Rapid warming in summer wet bulb globe temperature in china with human-induced climate change. J. Clim. 33, 5697–5711. https://doi.org/10.2196/10.1175/JCLI-D-19-0492.1.
Li, K., Amatus, G., 2020. Spatiotemporal changes of heat waves and extreme temperatures in the main cities of China from 1955 to 2014. Nat. Hazards Earth Syst. Sci. 20, 1889–1901. https://doi.org/10.5194/nhess-20-1889-2020.
Lipiec, J., Doussan, C., Nosalewicz, A., Kondracka, K., 2013. Effect of drought and heat stresses on plant growth and yield: a review. Int. Agrophys. 27, 463–477. https://doi.org/10.2478/intag-2013-0017.
Liu, Z., Yang, X., Hubbard, K.G., Lin, X., 2012. Maize potential yields and yield gaps in the changing climate of northeast China. Glob. Chang. Biol. 18, 3441–3454. https://doi.org/10.1111/j.1365-2486.2012.02774.x.
Liu, Z., Hubbard, K.G., Lin, X., Yang, X., 2013a. Negative effects of climate warming on maize yield are reversed by the changing of sowing date and cultivar selection in Northeast China. Glob. Chang. Biol. 19, 3481–3492. https://doi.org/10.1111/gcb.12324.
Liu, Z., Yang, X., Chen, F., Wang, E., 2013b. The effects of past climate change on the northern limits of maize planting in Northeast China. Clim. Change 117, 891–902. https://doi.org/10.1007/s10584-012-0594-2.
Lobell, D.B., Hammer, G.L., Chenu, K., Zheng, B., Mclean, G., Chapman, S.C., 2015. The shifting influence of drought and heat stress for crops in Northeast Australia. Glob. Chang. Biol. 21, 4115–4127. https://doi.org/10.1111/gcb.13022.
Lobell, D.B., Schlenker, W., Costa-Roberts, J., 2011. Climate trends and global crop production since 1980. Science 333, 616–620. https://doi.org/10.1126/science.1204531.
Mahrookashani, A., Siebert, S., Hüging, H., Ewert, F., 2017. Independent and combined effects of high temperature and drought stress around anthesis on wheat. J. Agron. Crop Sci. 203, 453–463. https://doi.org/10.1111/jac.12218.
Manderscheid, R., Erbs, M., Weigel, H.-J., 2015. Key physiological parameters related to differences in biomass production of maize and four sorghum cultivars under drought and free air CO_2 enrichment. Procedia Environ. Sci. 29, 89–90. https://doi.org/10.1016/j.proenv.2015.07.174.
Matiu, M., Ankerst, D.P., Menzel, A., 2017. Interactions between temperature and drought in global and regional crop yield variability during 1961–2014. PLoS One 12, e0178339. https://doi.org/10.1371/journal.pone.0178339.
Mesbahzadeh, T., Mirakbari, M., Mohseni Saravi, M., Soleimani Sardoo, F., Miglietta, M. M., 2020. Meteorological drought analysis using copula theory and drought indicators under climate change scenarios (RCP). Meteorol. Appl. 27 https://doi.org/10.1002/met.1856.
Miao, C., Sun, Q., Duan, Q., Wang, Y., 2016. Joint analysis of changes in temperature and precipitation on the Loess Plateau during the period 1961–2011. Clim. Dyn. 47, 3221–3234. https://doi.org/10.1007/s00382-016-3022-x.
Miliauskienė, J., Sakalauskienė, S., Lazauskas, S., Povilaitis, V., Brazaitytė, A., Duchovskis, P., 2016. The competition between winter rape (C3) and maize (C4) plants in response to elevated carbon dioxide and temperature, and drought stress. Zemdirb. Agric. 103, 21–28. https://doi.org/10.13080/z-a.2016.103.003.
Mingyuan, Z., Pan, G., Yongbo, Y., 2016. Assessment model of drought and waterlogging with could model. Fuzzy Syst. Math. 30.
Panagopoulos, A., 2021. Water-energy nexus: desalination technologies and renewable energy sources. Environ. Sci. Pollut. Res. 28, 21009–21022. https://doi.org/10.1007/s11356-021-13332-8.
Panagopoulos, A., Haralambous, K.-J., Loizidou, M., 2019. Desalination brine disposal methods and treatment technologies - a review. Sci. Total Environ. 693, 133545 https://doi.org/10.1016/j.scitotenv.2019.07.351.
Paredes, P., Pereira, L.S., Almorox, J., Darouich, H., 2020. Reference grass evapotranspiration with reduced data sets: parameterization of the FAO Penman-Monteith temperature approach and the Hargeaves-Samani equation using local climatic variables. Agric. Water Manag. 240, 106210 https://doi.org/10.1016/j.agwat.2020.106210.
Pingya, T., Biying, L., 1985. Some suggestions on unified division of maize growth period. Tillage Cultiv. 04.
Qian, X., Qiu, B., Zhang, Y., 2019. Widespread decline in vegetation photosynthesis in Southeast Asia due to the prolonged drought during the 2015/2016 El Niño. Remote Sens. 11, 910. https://doi.org/10.3390/rs11080910.
Ray, D.K., West, P.C., Clark, M., Gerber, J.S., Prishchepov, A.V., Chatterjee, S., 2019. Climate change has likely already affected global food production. PLoS One 14, e0217148. https://doi.org/10.1371/journal.pone.0217148.
Sadegh, M., Ragno, E., AghaKouchak, A., 2017. Multivariate Copula Analysis Toolbox (MvCAT): describing dependence and underlying uncertainty using a Bayesian framework. Water Resour. Res. 53, 5166–5183. https://doi.org/10.1002/2016WR020242.
Sadegh, M., Moftakhari, H., Gupta, H.V., Ragno, E., Mazdiyasni, O., Sanders, B., Matthew, R., AghaKouchak, A., 2018. Multihazard scenarios for analysis of compound extreme events. Geophys. Res. Lett. 45, 5470–5480. https://doi.org/10.1029/2018GL077317.
Salvadori, G., De Michele, C., 2004. Frequency analysis via copulas: theoretical aspects and applications to hydrological events. Water Resour. Res. 40, 1–17. https://doi.org/10.1029/2004WR003133.
Salvadori, G., De Michele, C., 2010. Multivariate multiparameter extreme value models and return periods: a copula approach. Water Resour. Res. 46, 219–233. https://doi.org/10.1029/2009WR009040.
Sharma, S., Mujumdar, P., 2017. Increasing frequency and spatial extent of concurrent meteorological droughts and heatwaves in India. Sci. Rep. 7. https://doi.org/10.1038/s41598-017-15896-3.
Siebert, S., Webber, H., Zhao, G., Ewert, F., 2017. Heat stress is overestimated in climate impact studies for irrigated agriculture. Environ. Res. Lett. 12, 054023 https://doi.org/10.1088/1748-9326/aa702f.
Sillmann, J., Kharin, V.V., Zwiers, F.W., Zhang, X., Bronaugh, D., 2013. Climate extremes indices in the CMIP5 multimodel ensemble: Part 2. Future climate projections. J. Geophys. Res. Atmos. 118, 2473–2493. https://doi.org/10.1002/jgrd.50188.
Sun, Y., Zhang, X., Zwiers, F.W., Song, L., Wan, H., Hu, T., Yin, H., Ren, G., 2014. Rapid increase in the risk of extreme summer heat in Eastern China. Nat. Clim. Chang. 4, 1082–1085. https://doi.org/10.1038/nclimate2410.
Tursken, I.B., 2006. Type 2 uncertainty in knowledge representation and reasoning, in: Proceedings Joint 9th IFSA World Congress and 20th NAFIPS International Conference (Cat. No. 01TH8569), IEEE. pp. 1914–1919. ⟨https://doi.org/10.1109/NAFIPS.2001.944359⟩.
Wang, F., Wang, Z., Yang, H., Di, D., Zhao, Y., Liang, Q., Hussain, Z., 2020. Comprehensive evaluation of hydrological drought and its relationships with meteorological drought in the Yellow River basin, China. J. Hydrol. 584, 124751 https://doi.org/10.1016/j.jhydrol.2020.124751.
Wang, L., Chen, W., 2014. A CMIP5 multimodel projection of future temperature, precipitation, and climatological drought in China. Int. J. Climatol. 34, 2059–2078. https://doi.org/10.1002/joc.3822.

Wang, L., Liao, S., Huang, S., Ming, B., Meng, Q., Wang, P., 2018a. Increasing concurrent drought and heat during the summer maize season in Huang–Huai–Hai Plain, China. Int. J. Climatol. 38, 3177–3190. https://doi.org/10.1002/joc.5492.

Wang, R., Zhang, J., Guo, E., Li, D., Si, H., Si, A., 2018b. Spatiotemporal characteristics of drought and waterlogging during maize growing season in midwestern Jilin province for recent 55 years. J. Nat. Disasters 27, 186–197. https://doi.org/10.13577/j.jnd.2018.0122.

Wang, R., Zhao, C., Zhang, J., Guo, E., Li, D., Alu, S., Ha, S., Dong, Z., 2019. Bivariate copula function-based spatial–temporal characteristics analysis of drought in Anhui Province, China. Meteorol. Atmos. Phys. 131, 1341–1355. https://doi.org/10.1007/s00703-018-0640-3.

Wu, C., Zhou, L., Zhang, L., Jin, J., Zhou, Y., 2019. Precondition cloud algorithm and Copula coupling model-based approach for drought hazard comprehensive assessment. Int. J. Disaster Risk Reduct. 38, 101220 https://doi.org/10.1016/j.ijdrr.2019.101220.

Xiaogang, Y., Meng, W., Qingxin, K., Zhanbiao, W., 2015. Impacts of high temperature on maize production and adaptation measures in Northeast China. Chin. J. Appl. Ecol. 26, 186–198 (in Chinese).

Xiaoqing, W., Jian, L., Zhiyuan, W., 2015. Comparison of simulated and reconstructed temperature in China during the past 2000 years. Adv. Earth Sci. 30, 1318–1327 (in Chinese).

Xiuping, Z., 2014. Division of growth period and growth and development characteristics of maize. Tech. Advis. Anim. 04, 85 (in Chinese).

Yang, X., Gao, W., Shi, Q., Chen, F., Chu, Q., 2013. Impact of climate change on the water requirement of summer maize in the Huang-Huai-Hai farming region. Agric. Water Manag. 124, 20–27. https://doi.org/10.1016/j.agwat.2013.03.017.

Yang, X., Jin, X., Chu, Q., Pacenka, S., Steenhuis, T.S., 2021. Impact of climate variation from 1965 to 2016 on cotton water requirements in North China Plain. Agric. Water Manag. 243, 106502 https://doi.org/10.1016/j.agwat.2020.106502.

Yang, X.-L., Song, Z.-W., Wang, H., Shi, Q.-H., Chen, F., Chu, Q.-Q., 2012. Spatio-temporal variations of winter wheat water requirement and climatic causes in Huang-Huai-Hai Farming Region. Chin. J. Eco Agric. 20, 356–362. https://doi.org/10.3724/sp.j.1011.2012.00356.

Yin, X., Olesen, J.E., Wang, M., Öztürk, I., Zhang, H., Chen, F., 2016b. Impacts and adaptation of the cropping systems to climate change in the Northeast Farming Region of China. Eur. J. Agron. 78, 60–72. https://doi.org/10.1016/j.eja.2016.04.012.

Yin, X.G., Jabloun, M., Olesen, J.E., Öztürk, I., Wang, M., Chen, F., 2016a. Effects of climatic factors, drought risk and irrigation requirement on maize yield in the Northeast Farming Region of China. J. Agric. Sci. 154, 1171–1189. https://doi.org/10.1017/S0021859616000150.

You, Q., Yan, L., Zhao, L., 2018. Probability analysis of the water table and driving factors using a multidimensional copula function. Water 10, 472. https://doi.org/10.3390/w10040472.

Zandalinas, S.I., Mittler, R., Balfagón, D., Arbona, V., Gómez-Cadenas, A., 2018. Plant adaptations to the combination of drought and high temperatures. Physiol. Plant. 162, 2–12. https://doi.org/10.1111/ppl.12540.

Zhang, F., Yang, X., Sun, S., Gao, J., Liu, Z., Zhang, Z., Liu, T., 2021. A spatiotemporal analysis of extreme agrometeorological events during selected growth stages of maize (Zea mays L.) from 1960 to 2017 in Northeast China. Theor. Appl. Climatol. 143, 943–955. https://doi.org/10.1007/s00704-020-03465-0.

Zhang, J., 2004. Risk assessment of drought disaster in the maize-growing region of Songliao Plain, China. Agric. Ecosyst. Environ. 102, 133–153. https://doi.org/10.1016/j.agee.2003.08.003.

Zhang, Q., Hu, Z., 2018. Assessment of drought during corn growing season in Northeast China. Theor. Appl. Climatol. 133, 1315–1321. https://doi.org/10.1007/s00704-018-2469-6.

Zhang, Q., Tang, J., Feng, Y.C., Zhang, Y.X., Cai, C.L., 2017. Determination of extreme high temperature thresholds before and after summer corn jointing stage in shandong based on accumulated temperature-yield model. Chin. J. Agrometeorol. 38, 795–800. https://doi.org/10.3969/j.issn.1000-6362.2017.12.006.

Zhang, Q.W., Zhang, Y.Z., Zhong, M., 2014. A cloud model based approach for multi-hierarchy fuzzy comprehensive evaluation of reservoir-induced seismic risk. Shuili Xuebao J. Hydraul. Eng. 45, 87–95. https://doi.org/10.13243/j.cnki.slxb.2014.01.012.

Zhao, J., Yang, X., Lv, S., Liu, Z., Wang, J., 2014. Variability of available climate resources and disaster risks for different maturity types of spring maize in Northeast China. Reg. Environ. Chang. 14, 17–26. https://doi.org/10.1007/s10113-013-0476-9.

Zheng-Jie, X.U., Zhang, Y.P., Hong-Sheng, S.U., 2014. Application of risk assessment on fuzzy comprehensive evaluation method based on the cloud model. J. Saf. Environ. (In Chinese).

Zhong, Q., Jiao, L., Zhi, L.I., Jiao, W., Chen, Y.N., 2019. Spatial and temporal changes of potential evapotranspiration and its attribution in the Bosten Lake Basin. Arid L. Geogr. (In Chinese).